

Vector Dark Matter in a $U(1)_X$ extended 2HDM

Nandini Das,^a Juhi Dutta,^{b,c} Dilip Kumar Ghosh,^a Santosh Kumar Rai^d

^a*School of Physical Sciences, Indian Association for the Cultivation of Science, 2A & 2B, Raja S.C. Mullick Road, Kolkata 700032, India*

^b*Homer L. Dodge Department of Physics and Astronomy, University of Oklahoma, Norman, OK 73019, USA*

^c*The Institute of Mathematical Sciences, 4th Cross St, CIT Campus, Tharamani, Chennai, Tamil Nadu, India, 600113*

^d*Regional Centre for Accelerator-based Particle Physics, Harish-Chandra Research Institute, A CI of Homi Bhabha National Institute, Chhatnag Road, Jhunsī, Prayagraj – 211019, India*

E-mail: nandinidas.rs@gmail.com, juhidutta@imsc.res.in,
tpdkg@iacs.res.in, skrai@hri.res.in

ABSTRACT: We investigate the possibility of having a vector boson dark matter in a $U(1)_X$ extended two-Higgs-doublet model (2HDM) setup. The gauge boson gains mass when a SM singlet complex scalar, which is charged under the dark $U(1)_X$ symmetry, acquires vacuum expectation value (vev). This scalar acts as the connection between the SM sector and DM via the Higgs portal. An additional exact charge conjugation symmetry inhibits the mixing of this gauge boson with the photon, thereby confirming the stability of DM. On the other hand, 2HDM with Type I Z_2 restriction can offer a non-standard Higgs in the lighter mass range. This freedom allows us to accommodate dark matter mass in the (40-60) GeV regime where the direct detection constraints are strongest. We study the dark matter phenomenology of such a model while taking care of all possible theoretical and experimental constraints.

Contents

1	Introduction	1
2	Model Setup	3
2.1	Scalar Sector	3
2.2	Yukawa Sector	6
2.3	Dark Sector	7
3	Constraints	9
3.1	Theoretical constraints	9
3.2	Experimental Constraints	9
4	Impact of theoretical constraints	11
5	Dark Matter Phenomenology	12
5.1	Relic constraint and Direct Detection	13
5.2	Indirect Detection	16
6	Discussion on Freeze-in prospect	17
7	Summary and Conclusions	19
8	Appendix	21
8.1	Quartic couplings in terms of physical parameters	21
8.2	Condition for Unitarity	22
8.3	Boltzmann equations	22

1 Introduction

The Standard Model (SM) is the most widely accepted description of the physics of electroweak and strong interactions. The recent discovery of the Higgs boson only strengthens its construction. While SM is extremely successful in explaining the particle interaction of the visible sector, it remains silent about the “invisible” component of the universe. From Fritz Zwicky’s observations of galaxy clusters [1], to Vera Rubin’s studies of galactic rotation curves [2], and the Bullet Cluster data from the Chandra X-ray Observatory [3, 4], multiple observations have confirmed the presence of a mysterious “dark” component of the universe, non-luminous and non-baryonic in nature. Supported by the aforementioned various hints of evidence

along with gravitational lensing and anisotropies of Cosmic Microwave Background Radiation (CMBR) [5], the dark matter (DM), supplying 26% of the energy budget of the universe, is a mystery yet to be unveiled. One of the known facts about DM is its current number density ($\Omega_{DM}h^2$), which has been measured by WMAP [6] and PLANCK [5] very precisely and is reported to be $\Omega_{DM}h^2 = 0.12 \pm 0.001$ at 68% confidence level. Other than that, DM in terms of interaction, mass, or nature is an unsolved puzzle. Though evidences only reveal its gravitational nature, exploring its particle origin is still an interesting and complementary possibility. From the analogy of the visible universe, if DM is considered an elementary particle, it should be connected to the SM by some interaction, most likely a weak interaction. Interestingly, weakly interacting particles of electroweak mass scale can be in thermal equilibrium with the SM particle bath in the early universe and can freeze out from the bath with a residual number density which matches the observed DM density of the universe. This is often referred to as the WIMP miracle [7] in the literature. Due to its detection prospects, WIMP is the most economical dark matter candidate to date. Multiple direct detection (DD) experiments like LUX-ZEPLIN (LZ) [8, 9], (the most stringent limit till now), PANDAX [10, 11], and XENONnT [12, 13] have explored and excluded wide ranges of parameter spaces. Futuristic experiments like the DARWIN [14] intend to probe further parameter spaces in the coming years. Current direct search experiments have stringently constrained WIMP DM scenarios, particularly scalar and fermionic DM, which have been extensively looked into in various beyond Standard Model (BSM) theories. However, vector DM candidates are relatively less explored. Vector DM has been studied mainly in the context of extensions of SM via the Higgs portal with extra scalars [15–18], including $SU(2)_N$ extensions [19–21], vector-like fermion portals [22], and Type II seesaw [23].

On the other hand, the two-Higgs-doublet model (2HDM) [24] is a very well-motivated extension of the SM. Beyond its minimal scalar sector with two $SU(2)_L$ Higgs doublets, which can provide sources of spontaneous CP violation [25], explain the fermion mass hierarchy, etc., it can also provide an alternate perspective towards dark matter modeling. However, except for the inert Higgs doublet model [26], where the non-standard Higgs doublet does not acquire a VEV and can play the role of dark matter, only 2HDM can not have a natural dark matter candidate.

In this context, extended 2HDMs have been widely studied in the literature addressing the dark matter issue with fermion [27–31], pseudo-Nambu Goldstone boson [32–35] and scalar particle [36–45]. There have been a few searches [46, 47] following the effective field theory approach, where the phenomenology of fermion, scalar, and vector boson as DM candidates has been investigated. However, vector boson DM in a UV-complete 2HDM model framework has not been explored, and we focus on that scenario here.

In this work, we study the phenomenology of a vector dark matter candidate in the context of $U(1)_X$ extended Type I two Higgs doublet model (2HDM). Along with the

two $SU(2)_L$ Higgs doublets, an additional complex scalar is present in the particle spectrum, which is charged under an extra local $U(1)_X$ symmetry. This $U(1)_X$ is spontaneously broken by the VEV of the complex scalar while the DM gauge boson acquires mass by eating up the CP odd part of the complex scalar. The dark matter is stabilized by the imposition of an exact charge conjugation symmetry. Therefore, after electroweak symmetry breaking, the particle content consists of three CP-even Higgs fields h_1, h_2, h_3 , one CP-odd pseudoscalar A , a pair of charged Higgses H^\pm , and a gauge boson DM candidate Z' . Taking care of all possible theoretical and experimental constraints, we scrutinize our DM model parameter space under the existing and future direct detection experimental facilities. We provide the corresponding DM parameter space that can be probed soon by the current as well as future experiments, such as DARWIN.

This paper is organized as follows: We describe the model setup briefly in Section 2. The theoretical and experimental constraints are summarized in Section 3 and their impact on parameter space is shown in Section 4. The DM phenomenology of the model, considering freeze-out mechanism of production and its detectability, is shown in Section 5. The freeze-in prospect of the model is discussed in Section 6. Finally, we conclude in Section 7.

2 Model Setup

The SM gauge symmetry is extended with an additional $U(1)_X$ symmetry and in addition to the conventional content of the two Higgs doublet model (which extends the SM by an extra $SU(2)_L$ Higgs doublet), we have an extra singlet scalar which is charged under the new $U(1)_X$ symmetry. Note that the new gauge symmetry represents a dark sector, and the gauge boson, which arises from gauging the symmetry, acts as the dark matter candidate in the model. The model Lagrangian can be written as

$$\mathcal{L} = \mathcal{L}_{\text{Scalar}}^{\text{2HDM+Singlet}} + \mathcal{L}_{\text{Dark}}^{Z'} + \mathcal{L}_{\text{Yukawa}}^{\text{2HDM}} + \mathcal{L}_{\text{Gauge}}^{\text{2HDM}}$$

where the first term corresponds to the scalar sector of the model, the second term to the dark sector, the third term corresponds to the Yukawa sector, and the last term to the gauge sector of the SM. We describe each term in detail in the following.

2.1 Scalar Sector

The most general Lagrangian including two Higgs doublets and a $U(1)_X$ charged singlet scalar can be written as

$$\mathcal{L}_{\text{Scalar}}^{\text{2HDM+Singlet}} = \mathcal{L}_{\text{Kin}} - V(\Phi_1, \Phi_2, S)$$

where Φ_1, Φ_2 and S are the two Higgs doublets and complex singlet scalar, respectively.

The kinetic part of the Lagrangian comprises

$$\mathcal{L}_{\text{Kin}} = (D_\mu \Phi_1)^\dagger (D^\mu \Phi_1) + (D_\mu \Phi_2)^\dagger (D^\mu \Phi_2) + (D_\mu S)^* (D^\mu S)$$

where the covariant derivatives are as follows

$$\begin{aligned} D_\mu \Phi_1 &= \partial_\mu \Phi_1 + \frac{ig}{2} W_\mu^a \sigma^a \Phi_1 + \frac{ig'}{2} B_\mu \Phi_1 \\ D_\mu \Phi_2 &= \partial_\mu \Phi_2 + \frac{ig}{2} W_\mu^a \sigma^a \Phi_2 + \frac{ig'}{2} B_\mu \Phi_2 \\ D_\mu S &= \partial_\mu S + ig_x x_s Z'_\mu S. \end{aligned}$$

Here, g_x and x_s are the gauge coupling and charge of the scalar S under the dark $U(1)_X$, respectively. For simplicity, we choose $x_s = 1$ for the rest of the study.

The scalar potential is given by

$$\begin{aligned} V(\Phi_1, \Phi_2, S) &= m_{11}^2 (\Phi_1^\dagger \Phi_1) + m_{22}^2 (\Phi_2^\dagger \Phi_2) + m_{33}^2 (S^* S) - [m_{12}^2 (\Phi_1^\dagger \Phi_2) + \text{h.c.}] + \lambda_1 (\Phi_1^\dagger \Phi_1)^2 \\ &\quad + \lambda_2 (\Phi_2^\dagger \Phi_2)^2 + \lambda_S (S^* S)^2 + \lambda_3 (\Phi_1^\dagger \Phi_1) (\Phi_2^\dagger \Phi_2) + \lambda_4 (\Phi_1^\dagger \Phi_2) (\Phi_2^\dagger \Phi_1) \\ &\quad + \lambda_{S1} (\Phi_1^\dagger \Phi_1) (S^* S) + \lambda_{S2} (\Phi_2^\dagger \Phi_2) (S^* S) + \left\{ \frac{1}{2} \lambda_5 (\Phi_1^\dagger \Phi_2)^2 \right. \\ &\quad \left. + [\lambda_6 (\Phi_1^\dagger \Phi_1) + \lambda_7 (\Phi_2^\dagger \Phi_2) + \lambda_8 (S^* S)] \times (\Phi_1^\dagger \Phi_2) + \text{h.c.} \right\} \end{aligned}$$

where h.c. stands for the hermitian conjugate of the corresponding term. Following the Z_2 symmetry of Type I 2HDM, under which one of the Higgs doublets (in our case Φ_2) is odd, λ_6 , λ_7 , and λ_8 must vanish to avoid any explicit Z_2 breaking terms. However, m_{12}^2 can have non-zero values and appear as a soft Z_2 term. After electroweak symmetry breaking, the two scalar doublets Φ_1 and Φ_2 and singlet scalar S can be expanded around the vev 's as

$$\begin{aligned} \Phi_1 &= \begin{pmatrix} \phi_1^\dagger \\ \frac{1}{\sqrt{2}}(\rho_1 + v_1 + i\eta_1) \end{pmatrix}, \quad \Phi_2 = \begin{pmatrix} \phi_2^\dagger \\ \frac{1}{\sqrt{2}}(\rho_2 + v_2 + i\eta_2) \end{pmatrix}, \\ S &= \frac{1}{\sqrt{2}}(\rho_S + v_S + i\eta_S) \end{aligned}$$

where v_1, v_2 and v_S are the vev 's of the two Higgs doublets and singlet scalar, respectively. Minimizing the scalar potential around the vev , we obtain the following

relations,

$$\begin{aligned}
m_{11}^2 &= m_{12}^2 \frac{v_2}{v_1} - \lambda_1 v_1^2 - \frac{1}{2}(\lambda_3 + \lambda_4 + \lambda_5)v_2^2 - \frac{\lambda_{S1}}{2}v_S^2 \\
m_{22}^2 &= m_{12}^2 \frac{v_1}{v_2} - \lambda_2 v_2^2 - \frac{1}{2}(\lambda_3 + \lambda_4 + \lambda_5)v_1^2 - \frac{\lambda_{S2}}{2}v_S^2 \\
-m_{33}^2 &= \frac{\lambda_{S1}}{2}v_1^2 + \frac{\lambda_{S2}}{2}v_2^2 + \lambda_S v_S^2 .
\end{aligned}$$

The mass matrix of the charged scalars in the gauge eigen basis is given by

$$\mathcal{M}_{\pm}^2 = \begin{pmatrix} m_{12}^2 \frac{v_2}{v_1} - \frac{v_2^2}{2}(\lambda_4 + \lambda_5) & -m_{12}^2 + \frac{1}{2}v_1 v_2(\lambda_4 + \lambda_5) \\ -m_{12}^2 + \frac{1}{2}v_1 v_2(\lambda_4 + \lambda_5) & m_{12}^2 \frac{v_1}{v_2} - \frac{v_1^2}{2}(\lambda_4 + \lambda_5) \end{pmatrix} . \quad (2.1)$$

The field rotation of the charged scalars is given by

$$\begin{pmatrix} \phi_1^{\pm} \\ \phi_2^{\pm} \end{pmatrix} = \begin{pmatrix} \cos\beta & \sin\beta \\ \sin\beta & -\cos\beta \end{pmatrix} \begin{pmatrix} G^{\pm} \\ H^{\pm} \end{pmatrix}$$

where

$$\tan\beta = \frac{v_2}{v_1} . \quad (2.2)$$

One of the charged mass eigenstates becomes the Goldstone boson corresponding to the W^{\pm} boson. The mass eigenvalue of the other charged scalar is given by

$$m_{H^{\pm}}^2 = \left(\frac{m_{12}^2}{v_1 v_2} - \frac{1}{2}(\lambda_4 + \lambda_5) \right) (v_1^2 + v_2^2) . \quad (2.3)$$

The mass matrix of the CP-odd scalars in the gauge eigen basis is given by

$$\mathcal{M}_O^2 = \begin{pmatrix} m_{12}^2 \frac{v_2}{v_1} - \lambda_5 v_2^2 - m_{12}^2 + v_1 v_2 \lambda_5 & \\ m_{12}^2 + v_1 v_2 \lambda_5 & m_{12}^2 \frac{v_1}{v_2} - \lambda_5 v_1^2 \end{pmatrix} . \quad (2.4)$$

The relation between the gauge basis and mass basis of the CP odd scalars can be written as

$$\begin{pmatrix} \eta_1 \\ \eta_2 \end{pmatrix} = \begin{pmatrix} \cos\beta & \sin\beta \\ \sin\beta & -\cos\beta \end{pmatrix} \begin{pmatrix} G_0 \\ A \end{pmatrix} .$$

One of the pseudo-scalar acts as a Goldstone boson of the Z boson, whereas the mass eigenvalue of the other pseudo-scalar is given by

$$m_A^2 = \frac{(m_{12}^2 - \lambda_5 v_1 v_2)}{v_1 v_2} (v_1^2 + v_2^2) . \quad (2.5)$$

The mass matrix of the CP-even scalars is given by

$$\mathcal{M}_E^2 = \begin{pmatrix} m_{12}^2 \frac{v_2}{v_1} + 2\lambda_1 v_1^2 & -m_{12}^2 + \lambda_{345} v_1 v_2 & \lambda_{S1} v_1 v_S \\ -m_{12}^2 + \lambda_{345} v_1 v_2 & m_{12}^2 \frac{v_1}{v_2} + 2\lambda_2 v_2^2 & \lambda_{S2} v_2 v_S \\ \lambda_{S1} v_1 v_S & \lambda_{S2} v_2 v_S & 2\lambda_s v_S^2 \end{pmatrix} \quad (2.6)$$

where

$$\lambda_{345} = \lambda_3 + \lambda_4 + \lambda_5.$$

The CP even gauge eigenstates can be written as

$$\begin{pmatrix} \rho_1 \\ \rho_2 \\ \rho_S \end{pmatrix} = \begin{pmatrix} c_{\alpha_1} c_{\alpha_2} & -s_{\alpha_1} c_{\alpha_3} - c_{\alpha_1} s_{\alpha_2} s_{\alpha_3} & s_{\alpha_1} s_{\alpha_3} - c_{\alpha_1} c_{\alpha_3} s_{\alpha_2} \\ c_{\alpha_2} s_{\alpha_1} & c_{\alpha_1} c_{\alpha_3} - s_{\alpha_1} s_{\alpha_2} s_{\alpha_3} & -(c_{\alpha_1} s_{\alpha_3} + c_{\alpha_3} s_{\alpha_1} s_{\alpha_2}) \\ s_{\alpha_2} & c_{\alpha_2} s_{\alpha_3} & c_{\alpha_2} c_{\alpha_3} \end{pmatrix} \begin{pmatrix} h_1 \\ h_2 \\ h_3 \end{pmatrix} \quad (2.7)$$

where h_1, h_2 and h_3 are the mass eigenstates and $\alpha_1, \alpha_2, \alpha_3$ are the mixing angles in the CP-even Higgs sector. For our future references, we denote the 3×3 rotation matrix shown in eq.2.7 as \mathcal{R} , whose elements will play a crucial role in various Higgs couplings. The quartic couplings can be written in terms of the physical parameters (mass, mixing angles and vev). The expressions are given in Appendix 8.1. After trading off the three unphysical mass parameters by using the minimization conditions, we are left with the following set of free parameters

$$\{m_{h_1}, m_{h_2}, m_{h_3}, m_A, m_{H^\pm}, \sin \alpha_1, \sin \alpha_2, \sin \alpha_3, \tan \beta, m_{12}^2, v_S\} \quad (2.8)$$

where $m_{h_1}, m_{h_2}, m_{h_3}$ are mass eigenvalues of the CP-even neutral scalars, m_A and m_{H^\pm} are the mass eigenvalues for the CP-odd neutral scalar and the singly charged scalar respectively.

2.2 Yukawa Sector

For a general 2HDM, where no Z_2 symmetry is imposed on the Lagrangian, we can write the Yukawa terms of the Lagrangian as

$$\begin{aligned} -\mathcal{L}_{\text{Yukawa}} = & \overline{Q}_{Li}(Y_{1ij}^d \Phi_1 + Y_{2ij}^d \Phi_2) d_{Rj} + \overline{Q}_{Li}(Y_{1ij}^u \tilde{\Phi}_1 + Y_{2ij}^u \tilde{\Phi}_2) u_{Rj} \\ & + \overline{L}_{Li}(Y_{1ij}^\ell \Phi_1 + Y_{2ij}^\ell \Phi_2) e_{Rj} + h.c. \end{aligned}$$

where Y_α^f corresponds to the Yukawa couplings of f ($f = u, d, \ell$) type fermions to Φ_α ($\alpha = 1, 2$) Higgs doublet and i and j stand for fermion generation indices. After imposition of the Z_2 symmetry of Type I 2HDM to our Yukawa Lagrangian, the fermions only couple to the second Higgs doublet (Φ_2), which is dominated by the SM Higgs component in the mass basis. The corresponding Lagrangian for Type I

2HDM is

$$-\mathcal{L}_{\text{Yukawa}}^{2HDM} = \overline{Q}_{Li} Y_{2ij}^d \Phi_2 d_{Rj} + \overline{Q}_{Li} Y_{2ij}^u \tilde{\Phi}_2 u_{Rj} + \overline{L}_{Li} Y_{2ij}^\ell \Phi_2 e_{Rj} + h.c. \quad (2.9)$$

In the mass basis of Higgs and fermions, the Lagrangian can be written as [24]

$$\begin{aligned} -\mathcal{L}_{\text{Yuk}} = & - \sum_{f=u,d,\ell} \frac{m_f}{v} (\xi_{h_i}^f \bar{f} f h_i + -i \xi_A^f \bar{f} \gamma_5 f A) - \left(\frac{\sqrt{2} V_{ud}}{v} \bar{u} (m_u \xi_A^u P_L + m_d \xi_A^d P_R) d H^+ \right) \\ & + \frac{\sqrt{2} m_\ell \xi_A^\ell}{v} \bar{\nu}_L \ell_R H^+ + \text{H.c.} \end{aligned}$$

where m_f stands for fermion mass. The modified reduced coupling factors of the CP even Higgses to the fermions, $\xi_{h_i}^f$ are defined as [48]:

$$\xi_{h_i}^f = \frac{\mathcal{R}_{i2}}{\sin \beta} \quad (2.10)$$

where i runs from 1 to 3, corresponding to three CP even Higgses. \mathcal{R}_{i2} ($i = 1, 2, 3$) are the elements of the rotation matrix in the CP-even Higgs sector as shown in eq. 2.7. The reduced couplings of the CP odd scalar (ξ_A^f) and the charged scalar to the fermions are the same as the standard Type I 2HDM [24]. The alignment limit for this extended version of 2HDM is $\{\beta - (\alpha_1 + \text{sgn}(\alpha_2)\alpha_3)\} \rightarrow \pi/2$ for the case where h_2 acts as the SM-like Higgs boson. In the limit $\sin \alpha_2 \rightarrow 0$ & $\sin \alpha_3 \rightarrow 0$, the CP even reduced couplings return to the standard Type I 2HDM couplings.

2.3 Dark Sector

The $U(1)_X$ symmetric Lagrangian is invariant under $Z_2^{(A)} \times Z_2^{(B)}$ symmetry [15] which are defined as follows

$$Z_2^{(A)} : \quad Z'_\mu \rightarrow -Z'_\mu, S \rightarrow S^*, \quad Z_2^{(B)} : \quad Z'_\mu \rightarrow -Z'_\mu, S \rightarrow -S^*$$

This is also referred to as dark charge conjugation symmetry [49]. Demanding this charge conjugation symmetry to be exact ensures the stability of the vector boson Z' . In the presence of the dark conjugation symmetry, which prevents the mixing between Z'_μ with B_μ, W_μ^3 , the neutral gauge boson mass matrix is given by

$$M_{VZ}^2 = \begin{pmatrix} g^2 \frac{v^2}{4} & -gg' \frac{v^2}{4} & 0 \\ -gg' \frac{v^2}{4} & g'^2 \frac{v^2}{4} & 0 \\ 0 & 0 & g_x^2 v_S^2 \end{pmatrix}. \quad (2.11)$$

Upon diagonalizing the matrix, the eigenvalues are 0, $\frac{(g^2+g'^2)v^2}{2}$, $g_x^2 v_S^2$ representing the massless photon, the massive Z boson and the massive Z' boson. The Z' boson

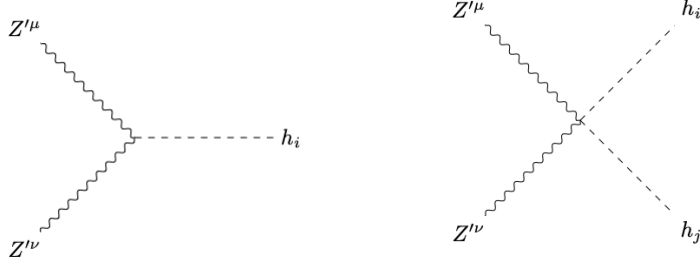


Figure 1. Relevant trilinear and quartic vertices of vector DM candidate Z' .

constitutes the vector DM candidate such that

$$m_{Z'} = g_x v_S \quad (2.12)$$

where $m_{Z'}$ is the mass of the Z' vector boson DM candidate. In our analysis, we treat $m_{Z'}$ and g_x as free parameters. For the remainder of the study, we define the DM mass as m_{DM} , where $m_{DM} = m_{Z'}$. Consequently, incorporating the dark sector, the model comprises twelve free parameters, which are listed as follows:

$$m_{h_1}, m_{h_2}, m_{h_3}, m_{H^\pm}, m_A, m_{12}^2, \tan \beta, \sin \alpha_1, \sin \alpha_2, \sin \alpha_3, m_{DM}, g_x \quad (2.13)$$

One of the parameters, m_{h_2} , which will be identified as the SM-like Higgs boson, is fixed at the experimentally observed value of 125 GeV. We assume degeneracy among h_1, H^\pm , and A to further reduce the number of free parameters. This choice of degeneracy is motivated by constraints from electroweak precision measurements.

A vector boson as dark matter interacts with the SM sector via the Higgses. The vertex factors for the relevant trilinear and quartic couplings of the dark matter are as follows

$$\begin{aligned} \lambda_{h_i Z' Z'} &= 2g_x^2 v_S \mathcal{R}_{i3} \\ \lambda_{Z' Z' h_i h_j} &= 2g_x^2 \mathcal{R}_{i3} \mathcal{R}_{j3} \end{aligned} \quad (2.14)$$

where \mathcal{R}_{ij} ($i, j = 1, 2, 3$) are the elements of the rotation matrix in the CP-even Higgs sector as shown in eq. 2.7.

3 Constraints

3.1 Theoretical constraints

Constraints from boundedness-from-below conditions

The boundedness-from-below (BFB) conditions are crucial to ensure the positivity of the scalar potential, i.e, $V(\Phi_1, \Phi_2, S) \geq 0$ for large values of the fields. Using copositivity and Sylvester criterion [50], the necessary and sufficient BFB conditions are,

$$\begin{aligned} \lambda_1 \geq 0, \quad \lambda_2 \geq 0, \quad \lambda_S \geq 0, \quad \lambda_3 + \lambda_4 - |\lambda_5| + 2\sqrt{\lambda_1 \lambda_2} \geq 0, \quad \lambda_3 + 2\sqrt{\lambda_1 \lambda_2} \geq 0, \\ \lambda_{S1} + 2\sqrt{\lambda_1 \lambda_S} \geq 0, \quad \lambda_{S2} + 2\sqrt{\lambda_2 \lambda_S} \geq 0, \\ 2\sqrt{2\lambda_1 \lambda_2 \lambda_S} + \lambda_{S1}\sqrt{2\lambda_2} + \lambda_{S2}\sqrt{2\lambda_1} + (\lambda_3 + \lambda_4 - |\lambda_5|)\sqrt{2\lambda_S} \\ + \sqrt{2(\lambda_{S1} + 2\sqrt{\lambda_1 \lambda_S})(\lambda_{S2} + 2\sqrt{\lambda_2 \lambda_S})((\lambda_3 + \lambda_4 - |\lambda_5|) + 2\sqrt{\lambda_1 \lambda_2})} \geq 0. \end{aligned}$$

In the limit where $\lambda_s \rightarrow 0$, $\lambda_{S1} \rightarrow 0$ and $\lambda_{S2} \rightarrow 0$, the conditions reduce to the BFB conditions of standard 2HDM [24].

Constraints from Unitarity

The unitarity constraints for this model set up are as follows

$$\lambda_3 + \lambda_4 < 8\pi, \quad \lambda_3 - \lambda_4 < 8\pi, \quad \lambda_3 + \lambda_5 < 8\pi, \quad \lambda_3 - \lambda_5 < 8\pi, \quad (3.1)$$

$$\lambda_1 + \lambda_2 \pm \sqrt{(\lambda_1 - \lambda_2)^2 + \lambda_4^2} < 8\pi, \quad \lambda_1 + \lambda_2 \pm \sqrt{(\lambda_1 - \lambda_2)^2 + \lambda_5^2} < 8\pi, \quad (3.2)$$

$$\lambda_3 + 2\lambda_4 \pm 3\lambda_5 < 8\pi, \quad 2\lambda_S < 8\pi, \quad \lambda_{S1} < 8\pi, \quad \lambda_{S2} < 8\pi. \quad (3.3)$$

The aforementioned conditions corresponding to charge-neutral scatterings can not be written in a closed analytical form. Hence, we estimate them numerically and provide the required expressions in the Appendix 8.2. In the limit $\lambda_s \rightarrow 0$, $\lambda_{S1} \rightarrow 0$ and $\lambda_{S2} \rightarrow 0$, the above conditions simplify to the most stringent condition of the standard 2HDM [24] as shown:

$$3(\lambda_1 + \lambda_2) \pm \sqrt{9(\lambda_1 - \lambda_2)^2 + (2\lambda_3 + \lambda_4)^2} < 8\pi \quad (3.4)$$

3.2 Experimental Constraints

The 2HDM faces stringent constraints from experimental data from flavor physics, Higgs boson searches, precision measurements of oblique parameters, as well as dark matter and collider constraints from experiments. We discuss each of these constraints below:

Constraints from flavor physics

Data from the heavy flavor physics experiments are very useful in constraining the 2HDM parameter space. To constrain the model parameter space, we use the following heavy flavour physics observable: rare B-meson decays ($B \rightarrow X_s \gamma$ [51], $B_s \rightarrow \mu^+ \mu^-$ [52, 53], $B^\pm \rightarrow \tau^\pm \nu$ [54]) and neutral meson mixing depending on the different types of 2HDM. In Type I 2HDM, low $\tan \beta < 3$ regions are stringently constrained from $B_s \rightarrow \mu^+ \mu^-$ and ΔM_s [55–57] while for large values of $\tan \beta$ the bounds on charged Higgs masses from flavor physics are relaxed. For Type II 2HDM there exists a stringent bound on charged Higgs mass of $m_{H^\pm} \geq 650$ GeV from $Br(B \rightarrow X_s \gamma)$ [58] while the bound is weaker for Type I 2HDM and relaxes to $m_{H^\pm} \geq 80$ GeV. As the charged Higgs sector in our case remains the same as 2HDM, with no new decay modes, we ensure that the bounds from Type I 2HDM are used for the study.

Constraints from Higgs Boson searches

The Higgs sector of 2HDM has been extensively searched at colliders including LEP and LHC. From searches of pair-produced charged Higgs bosons at LEP in the context of 2HDM, masses below 80 GeV for the Type II scenario and 72.5 GeV for the Type I scenario are excluded [59]. However, in Type I 2HDM, $m_{H^\pm} < 200$ GeV for $\tan \beta < 10$ are constrained from $H^\pm \rightarrow \tau^\pm \nu$ searches [57]. Therefore, $\tan \beta \geq 10$ is a safe choice to evade these collider constraints.

For the neutral Higgses, we ensure that the second CP-even Higgs, h_2 is the SM-like Higgs such that $m_{h_2} = 125.25 \pm 0.17$ GeV [60]. The invisible branching of the SM-like Higgs to a dark matter pair is bounded from ATLAS and CMS as below

$$\begin{aligned} \text{BR}(h_2 \rightarrow Z' Z') &\leq 0.07_{-0.022}^{+0.030} \text{ (ATLAS) [61]} \\ &\leq 0.15 \text{ (CMS) [62]}. \end{aligned}$$

For a vector DM as in our case, the invisible decay width of the SM-like Higgs h_2 is given by

$$\Gamma(h_2 \rightarrow Z' Z') = \frac{g_x^2 m_{h_2} (\cos \alpha_2 \sin \alpha_3)^2}{32\pi x_{Z'}^2} (1 - 4x_{Z'}^2 + 12x_{Z'}^4) \sqrt{1 - 4x_{Z'}^2}, \quad (3.5)$$

where $x_{Z'}^2 = \frac{m_{Z'}^2}{m_{h_2}^2}$. We choose appropriate values for the mixing angles, $\sin \alpha_{1,2,3}$, to ensure that the SM-like 125 GeV Higgs invisible branching ratio is below the current limits from LHC.

We now discuss the constraints from collider searches of the neutral Higgses. The constraints from direct searches of non-standard Higgses, particularly, the $H \rightarrow \tau\tau$ searches, are the most stringent constraint in Type II 2HDM for large $\tan \beta$ [63]. However, Type I 2HDM is free from such stringent constraints. Recent results from

Run 2 of LHC show constraints for heavy Higgs masses beyond ~ 250 GeV [63] mainly via the heavy Higgs decaying to two SM-like Higgses or via searches of the pseudoscalar Higgs A decaying to a Z boson and SM Higgs. However, lighter non-standard Higgses remain free from these constraints. Further, throughout the work, we choose the heavier CP-even Higgs h_3 to be dominantly singlet-like via the choice of mixing angles, and hence it remains free from di-Higgs and $A \rightarrow Zh$ searches.

Constraints from oblique parameters

The mass differences of the components of the same multiplet can contribute to oblique parameters, leading to deviations from standard measured values of S , T and U where $S = 0.02 \pm 0.1$, $T = 0.07 \pm 0.12$, and $U = 0.00 \pm 0.09$ [64] and the model predictions of STU parameters are obtained from [65, 66]. As the dark matter analysis is not sensitive to these mass differences, we choose the particles from the same multiplet to be almost degenerate. Therefore, we choose degenerate masses for the non-standard neutral scalar h_1 , pseudoscalar A , and the charged Higgs H^\pm for the rest of the study.

In addition to the above, we consider the constraints from dark matter observables. We discuss these constraints and their impact on the model parameter space in Sec 5.

4 Impact of theoretical constraints

In this section, we show the effect of the theoretical constraints on the model parameter space. Here we scan over a wide range of Higgs masses without imposing any experimental constraints. Our scan range is as follows

$$\begin{aligned} m_{h_1} = m_{h^\pm} = m_A &\in \{80, 1000\}, \quad m_{h_3} \in \{200, 1000\}, \quad \tan \beta \in \{1, 100\}, \\ \sin \alpha_1 &\in \{0.001, 1\}, \quad \sin \alpha_2 \in \{0.001, 1\}, \quad \sin \alpha_3 \in \{0.001, 1\}, \\ g_x &\in \{0.1, 1\}, \quad m_{\text{DM}} \in \{10, 1000\}, \quad m_{12}^2 \in \{10, 1000\} \end{aligned}$$

The parameters of 2HDM, which are important for the dark matter dynamics, are the mass scale of the non-standard Higgs doublet and $\tan \beta$. As the first Higgs works as a mediator between DM and SM particles, this mass scale gives us control over the light DM mass range. However, the effect of $\tan \beta$ is implicit. Being the ratio of the *vevs* of two Higgs doublets, $\tan \beta$ controls the behavior of the two Higgs bosons when $\sin \alpha_i$'s are small. As the couplings of the SM Higgs to the fermions depend on the $\tan \beta$ parameter, the choice of $\tan \beta$ is important. We therefore show the allowed parameter space from theoretical constraints in the $\tan \beta$ vs m_{h_1} plane. We find out that though vacuum stability conditions are not very restrictive, conditions from unitarity exclude a significant amount of the current parameter space. Another important parameter of 2HDM is m_{12}^2 . In Fig.2, we show the allowed parameter space from unitarity in the aforementioned plane while the corresponding m_{12}^2 is shown by

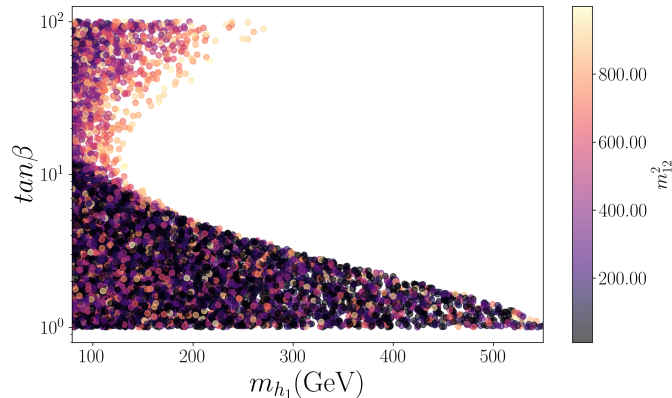


Figure 2. Parameter space in m_{h_1} vs $\tan\beta$ plane allowed from unitarity and BFB conditions.

the colourbar. The maximum value of m_{h_1} is ~ 700 GeV and values of $\tan\beta > 10$ is constrained for mass $m_{h_1} > 100$ GeV. As our dark matter analysis mainly focuses on the lower ranges of dark matter, it necessitates a lighter Higgs. Therefore, we choose a mass range of $80 - 120$ GeV for m_{h_1} and $\tan\beta = 10$.

5 Dark Matter Phenomenology

Now we move to the dark matter phenomenology of our model. Due to the imposition of an exact dark charge conjugation symmetry, Z' can not interact with the photon and the Z boson. The only connection it has with SM is via the Higgs portal. However, for DM freeze-out, the necessary condition is that DM has to be in thermal equilibrium with the bath in the early universe. The main parameters which control the thermalisation of DM are the cross quartic couplings $\lambda_{S1}, \lambda_{S2}$ and the $U(1)_X$ gauge coupling, g_x . Their importance can be understood from the representative diagrams shown in Fig.3. The first two diagrams mainly depend on the gauge coupling, while the last one is dictated by λ_{S2} only. The first diagram corresponds to a process where DM-SM particle interaction is mediated by the scalar mass eigenstates (h_1, h_2, h_3) and vice versa. The other two diagrams show a process where DM thermalises with S singlet scalar (dominantly h_3) for order one $U(1)_X$ gauge coupling, which further interacts with the SM Higgs by quartic couplings. Our choice of $g_x \in [0 - 1]$ keeps Z' in equilibrium with S . To ensure adequate mixing angles for our chosen parameters, we take λ_{S1} and λ_{S2} to be greater than 10^{-4} . This choice provides sufficient interaction strength with the Higgs boson to maintain the dark matter in thermal equilibrium. Ensuring the thermalisation of DM in the current scenario, we explore the parameter space of our model and its detection aspects that satisfy the relic density constraint.

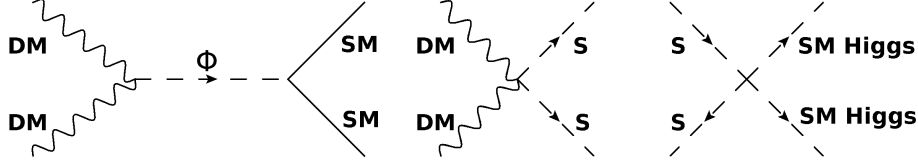


Figure 3. Diagrams for thermalisation of Z' . In the leftmost diagram, Φ denotes the 3 Higgs bosons h_1, h_2, h_3 in mass eigenstate.

5.1 Relic constraint and Direct Detection

The only thing we know about dark matter so far, based on the Λ CDM model, is its current density. The comoving number density of our considered DM species is governed by the following Boltzmann equation

$$\frac{dY_{Z'}}{dx} = \langle \sigma v \rangle_{Z'Z' \rightarrow XY} \frac{\beta s}{\mathcal{H} x} (Y_{Z'}^2 - Y_{Z'}^{eq2})$$

. Here $Y_{Z'}$ is defined as $n_{Z'}/s$, the ratio of number density of Z' to the entropy density (s) of the visible sector. $\langle \sigma v \rangle_{Z'Z' \rightarrow XY}$ is the velocity averaged cross section of the process $Z'Z' \rightarrow XY$ where X, Y stand for SM particles and the additional non-standard Higgses. $x = m_h/T$ where T is the temperature and $\beta = (1 + \frac{1}{3} \frac{d \ln g_s}{d \ln T})$ where g_s is entropy-associated degrees of freedom. The expression of Hubble expansion rate is given by

$$\mathcal{H} = \sqrt{\frac{\pi^2 g_{*\rho}}{90}} \frac{T^2}{M_{Pl}} \quad (5.1)$$

where $g_{*\rho}$ is the total number of relativistic degrees of freedom at temperature T and $M_{Pl} = 2.4 \times 10^{18}$ GeV. The relic density (Ωh^2) and direct detection cross-section for Z' have been calculated using **micrOMEGAs**. We have implemented the model in **FeynRules** and used the generated **calcHEP** [67] files in **micrOMEGAs** (v5.3.41) [68].

In the left panel of Fig. 4, we show the variation of relic density as a function of the DM. For this, we fix three Higgs masses ($m_{h_1}, m_{h_2}, m_{h_3}$) at 80 GeV, 125 GeV, and 500 GeV, respectively. Except for the SM Higgs mass, the two other masses are two representative values of the lighter and heavier mass regions in comparison to the SM Higgs mass. Since the annihilation channels are mediated by the Higgs boson, the corresponding resonances appear near $\sim m_h/2$, leading to a sharp drop in the relic density. The black dashed line shows the relic density measured by **PLANCK** [5]. The red and blue lines show the relic abundance for $g_x = 0.1$ and $g_x = 1.0$, respectively. Increased coupling results in a higher annihilation rate; therefore, more underabundant parameter space, which has been shown in the figure. Except for the resonances, the fall in the relic density after $m_{DM} = 80$ GeV and $m_{DM} = 500$ GeV are due to the opening of channels $Z'Z' \rightarrow h_1 h_1$ and $Z'Z' \rightarrow h_2 h_2$ respectively. In the right panel of Fig. 4, the $\tan \beta$ dependence of relic density has been shown.

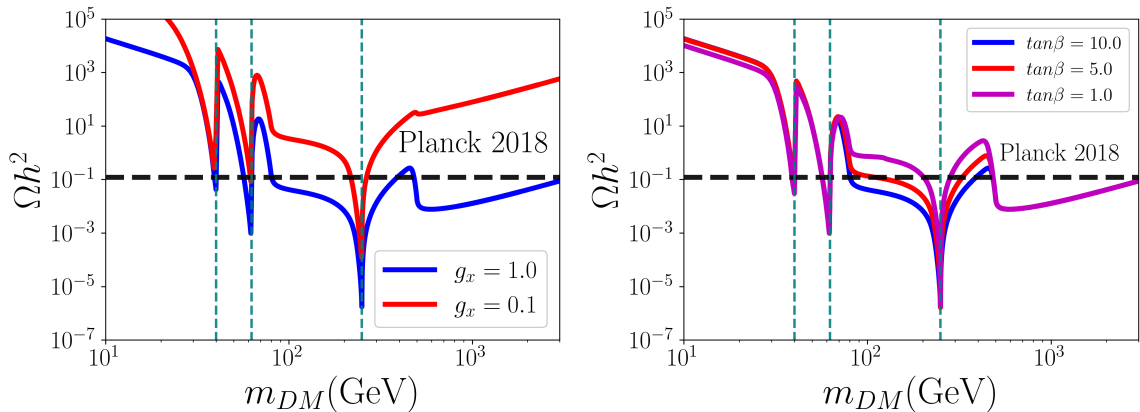


Figure 4. Relic abundance vs m_{DM} (GeV). The Higgs masses are fixed at $m_{h_1} = 80$ GeV, $m_{h_2} = 125$ GeV, $m_{h_3} = 500$ GeV. In the left panel, two values of g_x are considered when $\tan\beta = 10$. In the right panel, three values of $\tan\beta$ are considered when $g_x = 1.0$. The other parameters are fixed at $\sin\alpha_1 = 0.01$, $\sin\alpha_2 = 0.01$ and $\sin\alpha_3 = 0.01$.

With increasing $\tan\beta$, the decay width of $h_3(S)$ increases. This happens because the relevant Higgs trilinear couplings increase with $\tan\beta$, thereby increasing DM annihilation cross-section ($Z'Z' \rightarrow h_i h_j$). As a result, the under-abundant region increases with increased $\tan\beta$. Moreover, lower values of $\tan\beta$ alter the SM Higgs decay width. Therefore, we fix $\tan\beta = 10$ to strengthen the DM phenomenology and reduce the impact of Higgs constraints.

After discussing the basic nature of parameters, we now explore the relic density satisfied parameter space in light of DD experiments. The direct detection channel is mediated by the Higgs bosons as seen in Fig 5. Direct detection only considers the interaction of DM with nucleons, therefore quarks. In Type I 2HDM, only Φ_2 couples to quarks and S only couples to DM in the gauge basis. As a result, the direct detection cross-section significantly depends on the mixing angle between Φ_2 and S , denoted as α_3 , apart from the gauge coupling g_x . In Fig.6, we show a parameter space in m_{DM} vs σ_{SI} plane which gives the correct relic density within the 2σ range, consistent with current DD constraints. The left panel (right panel) corresponds to $\sin\alpha_3 = 0.001$ ($\sin\alpha_3 = 0.01$). With a smaller mixing angle, the cross-section falls proportionally, therefore, we can have a parameter space which can be probed in the far future, while a parameter space with a relatively larger mixing angle ($\sin\alpha_3 = 0.01$) is highly constrained by the current LZ limit. The dependence on g_x is shown by the color bar. Here we have plotted the DD cross section for DM mass range $m_{DM} \in [80, 1000]$ GeV. In the higher mass region ($m_{DM} \in [100, 1000]$), the DM annihilation can result in correct abundance by any combination of $h_3(S)$

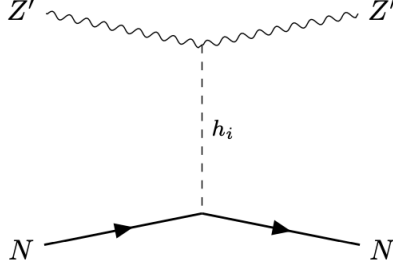


Figure 5. The Feynman diagram corresponding to the direct detection of the dark matter candidate Z' . Here, h_i ($i = 1, 2, 3$) refer to the Higgs bosons and N refers to a nucleon (proton or neutron).

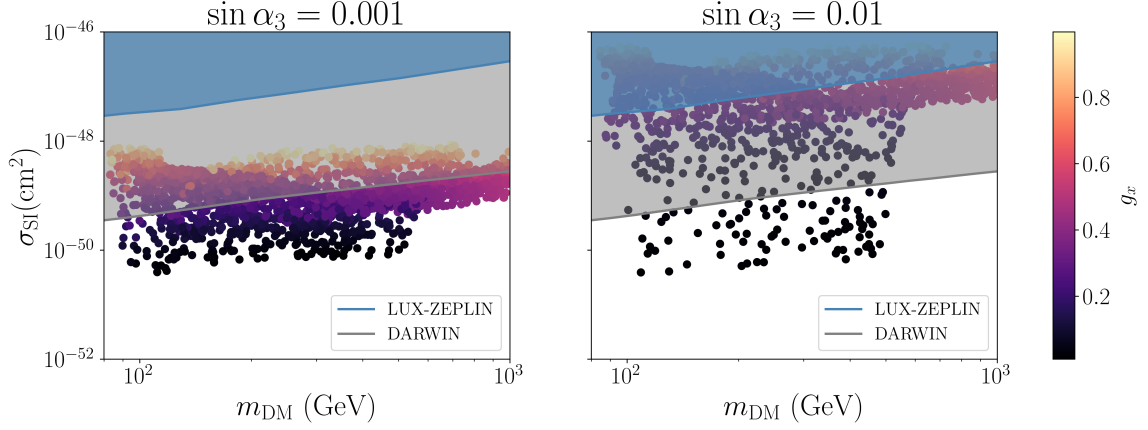


Figure 6. Parameter space with correct relic density in m_{DM} vs σ_{SI} plane for different values of mixing angles. The other Higgs doublet mass is varied between $m_{h_1} \in (80.0, 110.0)$ GeV, the singlet Higgs mass is varied between $m_{h_3} \in (200, 1000)$ GeV. The other parameters are fixed at the following values: $\tan \beta = 10$. For left panel, $\sin \alpha_3 = 0.001$ where as in the right panel, $\sin \alpha_3 = 0.01$.

resonance and opening of $Z'Z' \rightarrow h_i h_j$ channel. The dark colored points (black) with smaller values of DD cross-section are dominated by resonance annihilation. As a result, the dark points are allowed up to DM mass 500 GeV as shown in the figure, since the largest Higgs mass considered is 1000 GeV. The light colored points with relatively higher DD cross-sections satisfy the relic as more channels become available due to kinematics. However, in the range $[80, 100]$ GeV, due to the absence of a resonance, the process occurs only by opening the channel $Z'Z' \rightarrow h_1 h_1/h_2$. In the mass region ≤ 80 GeV, the SM Higgs resonance corresponds to a DM mass of 62.5 GeV, which is highly constrained from the Higgs invisible branching ratio. However, the presence of an additional Higgs with mass ≥ 80 GeV allows for a viable

DM in the mass range $[40, 60]$ GeV. In Fig. 7, we show the spin-independent cross section for the relic density satisfied points in this mass range. The blue shaded region shows the parameter space excluded by the LZ experiment. The grey shaded region shows the parameter space that can be probed by DARWIN soon.

5.2 Indirect Detection

Dark Matter can also be detected indirectly via its annihilation products in galaxies. The DM pair annihilates into SM and BSM final states via Higgs-mediated s-channel processes and quartic interactions of DM with Higgses, as shown in Fig. 3. In Fig. 8 we show the variation of the velocity-averaged DM annihilation cross section, $\langle\sigma v\rangle$, versus the dark matter mass m_{DM} with g_x in the colored palette. The plot is done for $\sin\alpha_3 = 0.01$ with an upper bound of $10^{-25} \text{cm}^3 \text{s}^{-1}$ to evade current limits from **Fermi-LAT**. The black dashed line denotes the thermal DM annihilation cross-section $10^{-26} \text{cm}^3 \text{s}^{-1}$ which corresponds to the required annihilation cross-section for the correct relic density.

We observe that for $m_{DM} < 100$ GeV, the total DM annihilation cross-section $\langle\sigma v\rangle$ is always less than $10^{-26} \text{cm}^3 \text{s}^{-1}$. For low DM masses, the dominant annihilation channels near the Higgs resonance regions are the SM channels, i.e, $b\bar{b}$, $c\bar{c}$, $\tau^+\tau^-$. For $m_{DM} > 90$ GeV, the bosonic channels W^+W^- , ZZ open up along with H^+H^- , $h_2 h_2$ and AA . While the SM branching modes are large near the Higgs resonance, particularly for $b\bar{b}$, it is safe from **Fermi-LAT** limits owing to the low $\langle\sigma v\rangle$ value. For heavier DM masses, the BSM channels AA, H^+H^-, W^+H^- ($i, j = 1, 2$) dominate over the SM channels and are safe from indirect detection limits from **Fermi-LAT**, as these channels are not constrained directly from data.

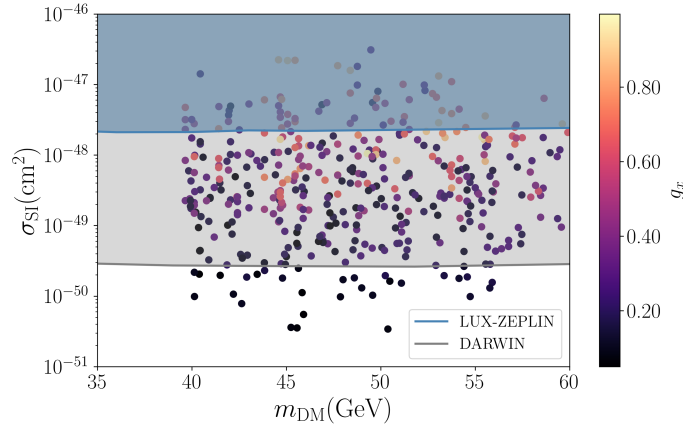


Figure 7. Relic density satisfied parameter space in m_{DM} vs σ_{SI} plane for lighter DM mass range.

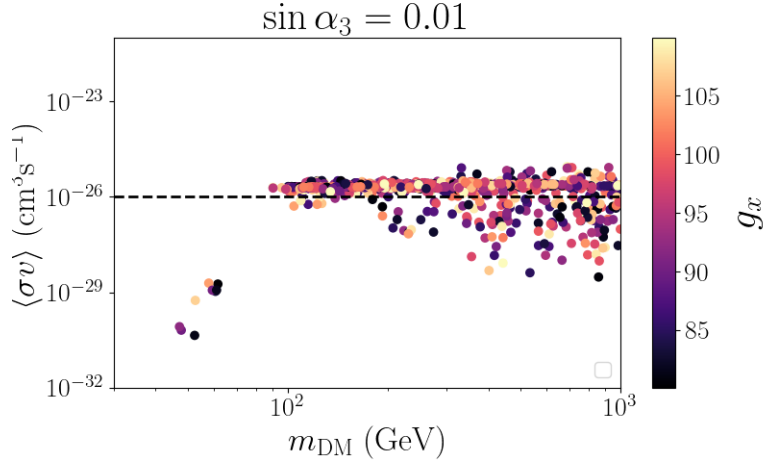


Figure 8. Relic density satisfied parameter space in annihilation cross section vs m_{DM} plane.

6 Discussion on Freeze-in prospect

While an $\mathcal{O}(1)$ gauge coupling makes the freeze-out production mechanism a natural candidate for DM generation, the continued non-observation of DM till recent times motivates us to look for a complementary approach. Assuming a very tiny gauge coupling for our case, one can still achieve a correct density of DM non-thermally [69]. Therefore, even with a negligible initial abundance, Z' can still be produced via decay and scattering of S (h_3) particles. As we shall consider very small mixing angles, the gauge and mass eigenstates will be almost the same ($S \sim h_3, \Phi_1 \sim h_1, \Phi_2 \sim h_2$), and therefore we will mention them interchangeably. S can be initially in thermal equilibrium with the SM bath via the quartic couplings with two Higgs doublets. Being directly coupled to S , the couplings of Z' to Φ_1 and Φ_2 are $\sin \alpha_i$ suppressed, therefore, their contribution to Z' abundance can be neglected. The relevant number density for the freeze-in scenario would be that of the S particle and DM Z' . We solve the two coupled Boltzmann equations mentioned in the appendix 8.3 to study the evolution of DM density. In Fig. 9, we present the evolution of comoving number densities of the above two species. The dashed lines correspond to a scenario where the extra light Higgs doublet is not present in the spectrum. Therefore, S only decays to DM as other decay channels to SM particles are suppressed by the mixing angle. Initially, S remains in thermal equilibrium via its interaction with the SM Higgs. After some time, it freezes out of equilibrium, but finally transfers its number density to the DM density as shown in the figure. Here, the mass of S is such that its decay to two SM Higgs is kinematically forbidden. But having Φ_1 as the light Higgs doublet in the spectrum provides an extra decay channel for S , thereby keeping S in thermal equilibrium throughout the whole period. This feature is visible in the solid lines of Fig. 9. In the available parameter space, where $m_S < 2m_{\Phi_2}$, the presence of

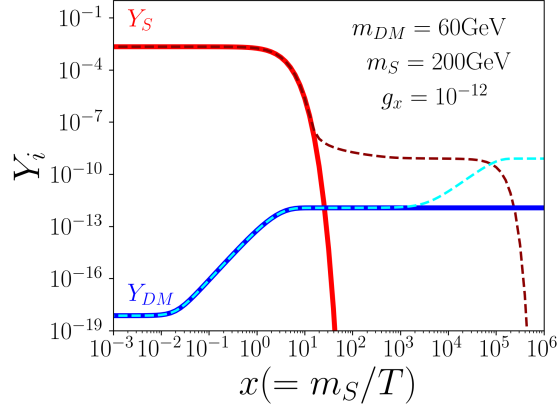


Figure 9. Evolution of comoving number density of DM and parent particle S . The dashed (solid) line corresponds to the scenario where decay of $S \rightarrow \Phi_1 \Phi_1$ is absent (present).

a light Φ_1 can stop freezing out of S , therefore keeping the relic density in the right ballpark. This can be considered as an advantage of having an extra light Higgs doublet in the spectrum. Therefore, we have safely considered S to be in thermal equilibrium, following which the Boltzmann equation of DM number density can be written as

$$\frac{dY_{\text{DM}}}{dx} = \frac{\langle \Gamma_{S \rightarrow \text{DM DM}} \rangle}{\mathcal{H}x} Y_S^{\text{eq}}(x) \quad (6.1)$$

where $x = m_S/T$. The DM number density in the present era is given by

$$\Omega_{\text{DM}} h^2 \simeq 2.755 \times 10^8 \frac{m_{\text{DM}}}{\text{GeV}} Y_{\text{DM}}^{\text{today}}. \quad (6.2)$$

The approximate expression of DM mass and mother particle S can be expressed as

$$m_{\text{DM}} = g_x v_S, \quad m_S \sim \sqrt{\lambda_S} v_S. \quad (6.3)$$

Combining these two equations, we have an approximate relation between the masses of the daughter DM and the mother particle referred to below

$$m_{\text{DM}} \sim \frac{m_S g_x}{\sqrt{\lambda_S}}. \quad (6.4)$$

Here we have performed a random scan to see what values of gauge coupling g_x and λ_S can produce correct relic abundance in the early universe. In Fig. 10, we show the parameter space available with correct relic abundance in the m_{DM} vs m_S plane. The corresponding dependence on g_x and λ_S is shown in the color bars in each corresponding plot. As expected, smaller values of g_x lead to lighter DM mass. Here we have shown the DM mass up to a few hundred keV. However, we can go down to a minimum of ~ 5 keV DM mass. Lower mass than that would be constrained from free-streaming length simulations [70, 71]. For satisfying the relic constraint, DM

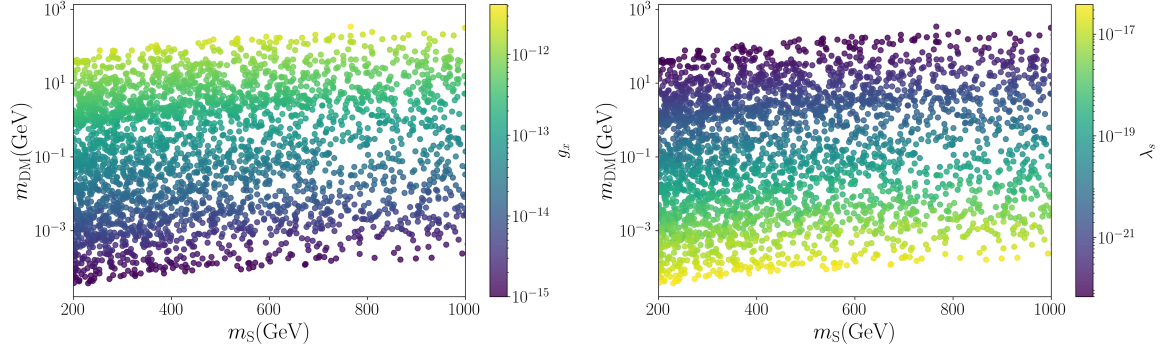


Figure 10. Parameter space with correct relic abundance in m_{DM} vs m_S plane. In the left (right) panel, the variation of gauge coupling g_x (self-coupling of S , λ_S) has been shown.

with mass 5 keV requires a g_x value of 5.495×10^{-16} (2.512×10^{-16}) for $m_S = 200$ GeV (1000 GeV). We can consider these values to be the lowest values of g_x for freeze-in production of dark matter.

7 Summary and Conclusions

In this work, we have explored the DM implications of the Universe in the context of the 2HDM. In a local $U(1)_X$ extended version of 2HDM, the extra gauge boson Z' can play the role of DM, where we have considered an exact dark charge conjugation symmetry to ensure the stability of the dark matter candidate. In addition to the standard two Higgs doublets, there is an extra complex scalar which is charged under the local $U(1)_X$. When this SM singlet complex scalar acquires a vev , the $U(1)_X$ symmetry is spontaneously broken, and the dark matter (DM) gains mass by eating up the CP odd degree of freedom of the $U(1)_X$ scalar. The DM interacts with the SM particles via the Higgs portal terms. We investigate the possibility of freeze-out of such a DM candidate and check its detectability under different direct detection and indirect detection experiments. In our analysis of the DM phenomenology in our model, we have considered all possible theoretical and experimental constraints applicable to such a scenario. Our choice of 2HDM parameters $\tan \beta$ and m_{h_1} (mass of the non-standard Higgs doublet) is motivated by experimentally favored parameter space. In terms of the DM analysis, the thermalisation of the DM in the early Universe is ensured by choosing an appropriate strength of interactions with the SM spectrum, which in our case gives $\lambda_{S2} \sim 10^{-4}$ and $g_x \in [0, 1]$. The DM number density in the current epoch is calculated using `micrOMEGAs`. The parameter space of our model, which satisfies the correct abundance of relic predicted by `PLANCK` within 2σ , can be probed in future DD experiments. A key feature of our model is

the existence of a viable parameter space in the dark matter mass range of $[40 - 60]$ GeV, even under strong direct detection limits. Generally, due to the resonance of the SM Higgs, some models allow dark matter masses around 62.5 GeV, which is severely restricted by the invisible branching ratio. In contrast to existing DM scenarios in the context of 2HDM, where DM densities are either underabundant (inert Higgs doublet models) in the mass range ≤ 90 GeV or very heavy (TeV mass), here we found a reasonable range of DM parameter space in the above mass range that is still allowed by DD experiments. Further, we also explore the case for tiny values of the gauge coupling (g_x) where the dark vector boson may become a non-thermal DM candidate. We present the region of allowed parameter space accommodating such a very light DM, with masses in the few keV to GeV region, produced via the freeze-in mechanism and satisfying the observed relic abundance.

Acknowledgements

ND would like to thank Anindya Datta, Rohan Pramanik, Tanmoy Kumar, and Koustav Mukherjee for discussions. ND acknowledges financial support from the CSIR, Government of India, through the NET Senior Research Fellowship (SRF), under Award File No. 09/080(1187)/2021-EMR-I. ND also acknowledges the hospitality of the Harish Chandra Research Institute, Prayagraj, India, where part of this work was carried out. JD acknowledges support from the OUHEP cluster at the University of Oklahoma and the Institute of Mathematical Sciences, India. SKR acknowledges the support from the Department of Atomic Energy (DAE), India, for the Regional Centre for Accelerator-based Particle Physics (RECAPP), Harish Chandra Research Institute.

8 Appendix

8.1 Quartic couplings in terms of physical parameters

The quartic couplings can be written in terms of physical parameters (mass, mixing angles, and vev) as

$$\begin{aligned}
\lambda_1 &= \frac{1}{2v_1^2} \{ m_{h_1}^2 \cos \alpha_1^2 \cos \alpha_2^2 + m_{h_2}^2 (\cos \alpha_3 \sin \alpha_1 + \cos \alpha_1 \sin \alpha_2 \sin \alpha_3)^2 + m_{h_3}^2 (\sin \alpha_1 \sin \alpha_3 \\
&\quad - \cos \alpha_1 \cos \alpha_3 \sin \alpha_2)^2 \} - m_{12}^2 \frac{v_2}{2v_1^3} \tag{8.1} \\
\lambda_2 &= \frac{1}{2v_2^2} \{ m_{h_1}^2 \sin \alpha_1^2 \cos \alpha_2^2 + m_{h_2}^2 (\cos \alpha_1 \cos \alpha_3 - \sin \alpha_1 \sin \alpha_2 \sin \alpha_3)^2 + m_{h_3}^2 (\cos \alpha_1 \sin \alpha_3 \\
&\quad + \sin \alpha_1 \sin \alpha_2 \cos \alpha_3)^2 \} - m_{12}^2 \frac{v_1}{2v_2^3} \\
\lambda_3 &= \frac{1}{v_1 v_2} \{ m_{h_1}^2 \sin \alpha_1 \cos \alpha_1 \cos \alpha_2^2 + m_{h_2}^2 (\cos \alpha_1 \sin \alpha_1 \sin \alpha_2^2 \sin \alpha_3^2 + \cos \alpha_3 \sin \alpha_2 \sin \alpha_3 \sin \alpha_1^2 \\
&\quad - \sin \alpha_2 \sin \alpha_3 \cos \alpha_3 \cos \alpha_1^2 - \sin \alpha_1 \cos \alpha_1 \cos \alpha_3^2) + m_{h_3}^2 (\cos \alpha_1 \cos \alpha_3^2 \sin \alpha_1 \sin \alpha_2^2 \\
&\quad + \cos \alpha_1^2 \cos \alpha_3 \sin \alpha_2 \sin \alpha_3 - \cos \alpha_3 \sin \alpha_1^2 \sin \alpha_2 \sin \alpha_3 - \cos \alpha_1 \sin \alpha_1 \sin \alpha_3^2) - m_{12}^2 \} \\
&\quad + \frac{2m_{H^\pm}^2}{(v_1^2 + v_2^2)} \\
\lambda_4 &= \frac{m_{12}^2}{v_1 v_2} + \frac{m_A^2 - 2m_{H^\pm}^2}{v_1^2 + v_2^2} \\
\lambda_5 &= \frac{m_{12}^2}{v_1 v_2} - \frac{m_A^2}{v_1^2 + v_2^2} \\
\lambda_s &= \frac{1}{2v_S^2} (m_{h_1}^2 \sin \alpha_2^2 + m_{h_2}^2 \cos \alpha_2^2 \sin \alpha_3^2 + m_{h_3}^2 \cos \alpha_2^2 \cos \alpha_3^2) \\
\lambda_{S1} &= \frac{1}{v_1 v_S} \{ m_{h_1}^2 \cos \alpha_1 \cos \alpha_2 \sin \alpha_2 - m_{h_2}^2 (\cos \alpha_2 \cos \alpha_3 \sin \alpha_1 \sin \alpha_3 + \cos \alpha_1 \cos \alpha_2 \sin \alpha_2 \sin \alpha_3^2) \\
&\quad + m_{h_3}^2 (\cos \alpha_2 \cos \alpha_3 \sin \alpha_1 \sin \alpha_3 - \cos \alpha_1 \cos \alpha_2 \cos \alpha_3^2 \sin \alpha_2) \} \\
\lambda_{S2} &= \frac{1}{v_2 v_S} \{ m_{h_1}^2 \cos \alpha_2 \sin \alpha_1 \sin \alpha_2 + m_{h_2}^2 (\cos \alpha_1 \cos \alpha_2 \cos \alpha_3 \sin \alpha_3 - \cos \alpha_2 \sin \alpha_1 \sin \alpha_2 \sin \alpha_3^2) \\
&\quad - m_{h_3}^2 (\cos \alpha_1 \cos \alpha_2 \cos \alpha_3 \sin \alpha_3 + \cos \alpha_2 \cos \alpha_3^2 \sin \alpha_1 \sin \alpha_2) \}
\end{aligned}$$

8.2 Condition for Unitarity

The amplitude matrix of charge neutral scatterings in all possible two particle states are presented below:

$$\mathcal{M} = \begin{pmatrix} 2\lambda_1 & \lambda_3 + \lambda_4 & \frac{\lambda_1}{2} & \frac{\lambda_3}{2} & \frac{\lambda_1}{2} & \frac{\lambda_3}{2} & \frac{\lambda_{s1}}{2} & \frac{\lambda_{s1}}{2} \\ \lambda_3 + \lambda_4 & 2\lambda_2 & \frac{\lambda_3}{2} & \frac{\lambda_2}{2} & \frac{\lambda_3}{2} & \frac{\lambda_2}{2} & \frac{\lambda_{s2}}{2} & \frac{\lambda_{s2}}{2} \\ \lambda_1 & \lambda_3 & \frac{3\lambda_1}{2} & \frac{1}{2}(\lambda_3 + \lambda_4 + \lambda_5) & \frac{\lambda_1}{2} & \frac{1}{2}(\lambda_3 + \lambda_4 - \lambda_5) & \frac{\lambda_{s1}}{2} & \frac{\lambda_{s1}}{2} \\ \lambda_3 & \lambda_2 & \frac{1}{2}(\lambda_3 + \lambda_4 + \lambda_5) & \frac{3\lambda_2}{2} & \frac{1}{2}(\lambda_3 + \lambda_4 - \lambda_5) & \frac{\lambda_2}{2} & \frac{\lambda_{s2}}{2} & \frac{\lambda_{s2}}{2} \\ \lambda_1 & \lambda_3 & \frac{\lambda_1}{2} & \frac{1}{2}(\lambda_3 + \lambda_4 - \lambda_5) & \frac{3\lambda_1}{2} & \frac{1}{2}(\lambda_3 + \lambda_4 + \lambda_5) & \frac{\lambda_{s1}}{2} & \frac{\lambda_{s1}}{2} \\ \lambda_3 & \lambda_2 & \frac{1}{2}(\lambda_3 + \lambda_4 - \lambda_5) & \frac{\lambda_2}{2} & \frac{1}{2}(\lambda_3 + \lambda_4 + \lambda_5) & \frac{3\lambda_2}{2} & \frac{\lambda_{s2}}{2} & \frac{\lambda_{s2}}{2} \\ \lambda_{s1} & \lambda_{s2} & \frac{\lambda_{s1}}{2} & \frac{\lambda_{s2}}{2} & \frac{\lambda_{s1}}{2} & \frac{\lambda_{s2}}{2} & 3\lambda_s & \lambda_s \\ \lambda_{s1} & \lambda_{s2} & \frac{\lambda_{s1}}{2} & \frac{\lambda_{s2}}{2} & \frac{\lambda_{s1}}{2} & \frac{\lambda_{s2}}{2} & \lambda_s & 3\lambda_s \end{pmatrix}$$

By demanding the largest eigen value of this matrix to be $\leq 8\pi$, we satisfy the conditions of unitarity.

8.3 Boltzmann equations

The comoving number density of S and DM are dictated by two coupled Boltzmann equations mentioned below

$$\begin{aligned} \frac{dY_{DM}}{dz} &= \frac{1}{z\mathcal{H}} \langle \Gamma_{S \rightarrow DM DM} \rangle Y_S(z) + \frac{4\pi^2}{45} M_{Pl} \frac{m_S}{1.66z^2} \langle \sigma v \rangle_{SS \rightarrow DM DM} Y_S^2(z) \\ \frac{dY_S}{dz} &= -\frac{1}{z\mathcal{H}} \langle \Gamma_{S \rightarrow DM DM} \rangle Y_S(z) - \sum_i \frac{1}{z\mathcal{H}} \langle \Gamma_{S \rightarrow \Phi_i \Phi_i} \rangle (Y_S(z) - Y_S^{eq}(z)) \\ &\quad - \frac{4\pi^2}{45} M_{Pl} \frac{m_S}{1.66z^2} (\langle \sigma v \rangle_{SS \rightarrow DM DM} Y_S^2(z) - \langle \sigma v \rangle_{SS \rightarrow HH} (Y_S^2(z) - Y_S^{eq2}(z))) \end{aligned}$$

where $Y_i = \frac{n_i}{s}$ and $i = 1, 2$. The thermal average of decay width and scattering cross-section are defined as

$$\begin{aligned} \langle \Gamma \rangle &= \Gamma \frac{K_1(z)}{K_2(z)} \\ \langle \sigma v \rangle &= \frac{z}{8m_S^5 K_2^2(z)} \int_{4m_S^2}^{\infty} \sigma(s) (s - 4m_S^2) \sqrt{s} K_1\left(\frac{\sqrt{s}}{T}\right) ds \end{aligned}$$

The relevant decay widths are mentioned below

$$\begin{aligned} \Gamma_{S \rightarrow Z' Z'} &= \frac{1}{32\pi} \frac{g_x^2 m_S^3}{m_{Z'}^2} \left(1 - \frac{4m_{Z'}^2}{m_S^2} + \frac{12m_{Z'}^4}{m_S^4}\right) \sqrt{1 - \frac{4m_{Z'}^2}{m_S^2}} \\ \Gamma_{S \rightarrow \Phi_i \Phi_i} &= \frac{(\lambda_{S_i} v_S)^2}{8\pi m_S} \sqrt{1 - \frac{4m_{\Phi_i}^2}{m_S^2}} \end{aligned}$$

The relevant cross sections are as follows

$$\sigma_{SS \rightarrow \Phi_i \Phi_i} = \frac{\lambda_{Si}^2}{16\pi s} \frac{\sqrt{s - 4m_{\Phi_i}^2}}{\sqrt{s - 4m_S^2}}$$

$$\sigma_{SS \rightarrow Z' Z'} = \frac{g_x^4}{16\pi s} \frac{\sqrt{s - 4m_{Z'}^2}}{\sqrt{s - 4m_S^2}} \left(3 + \frac{s^2}{4m_{Z'}^4} - \frac{s}{m_{Z'}^2} \right)$$

References

- [1] F. Zwicky, *Die Rotverschiebung von extragalaktischen Nebeln*, *Helv. Phys. Acta* **6** (1933) 110.
- [2] V.C. Rubin and W.K. Ford, Jr., *Rotation of the Andromeda Nebula from a Spectroscopic Survey of Emission Regions*, *Astrophys. J.* **159** (1970) 379.
- [3] R. Barrena, A. Biviano, M. Ramella, E.E. Falco and S. Seitz, *The dynamical status of the cluster of galaxies 1e0657-56*, *Astron. Astrophys.* **386** (2002) 816 [[astro-ph/0202323](#)].
- [4] D. Clowe, M. Bradac, A.H. Gonzalez, M. Markevitch, S.W. Randall, C. Jones et al., *A direct empirical proof of the existence of dark matter*, *Astrophys. J. Lett.* **648** (2006) L109 [[astro-ph/0608407](#)].
- [5] PLANCK collaboration, *Planck 2018 results. VI. Cosmological parameters*, *Astron. Astrophys.* **641** (2020) A6 [[1807.06209](#)].
- [6] WMAP collaboration, *Wilkinson Microwave Anisotropy Probe (WMAP) three year results: implications for cosmology*, *Astrophys. J. Suppl.* **170** (2007) 377 [[astro-ph/0603449](#)].
- [7] E.W. Kolb and M.S. Turner, *The Early Universe*, vol. 69, Taylor and Francis (5, 2019), [10.1201/9780429492860](#).
- [8] LZ collaboration, *The LUX-ZEPLIN (LZ) Experiment*, *Nucl. Instrum. Meth. A* **953** (2020) 163047 [[1910.09124](#)].
- [9] LZ collaboration, *First Dark Matter Search Results from the LUX-ZEPLIN (LZ) Experiment*, *Phys. Rev. Lett.* **131** (2023) 041002 [[2207.03764](#)].
- [10] PANDAX-II collaboration, *Dark Matter Results from First 98.7 Days of Data from the PandaX-II Experiment*, *Phys. Rev. Lett.* **117** (2016) 121303 [[1607.07400](#)].
- [11] PANDAX-II collaboration, *Dark Matter Results From 54-Ton-Day Exposure of PandaX-II Experiment*, *Phys. Rev. Lett.* **119** (2017) 181302 [[1708.06917](#)].
- [12] XENON collaboration, *Dark Matter Search Results from a One Ton-Year Exposure of XENON1T*, *Phys. Rev. Lett.* **121** (2018) 111302 [[1805.12562](#)].
- [13] XENON collaboration, *First Dark Matter Search with Nuclear Recoils from the XENONnT Experiment*, *Phys. Rev. Lett.* **131** (2023) 041003 [[2303.14729](#)].

- [14] DARWIN collaboration, *DARWIN: towards the ultimate dark matter detector*, *JCAP* **11** (2016) 017 [[1606.07001](#)].
- [15] Y. Farzan and A.R. Akbarieh, *VDM: A model for Vector Dark Matter*, *JCAP* **10** (2012) 026 [[1207.4272](#)].
- [16] O. Lebedev, H.M. Lee and Y. Mambrini, *Vector Higgs-portal dark matter and the invisible Higgs*, *Phys. Lett. B* **707** (2012) 570 [[1111.4482](#)].
- [17] S. Yaser Ayazi, M. Hosseini, S. Paktinat Mehdiabadi and R. Rouzbehi, *Vector dark matter and LHC constraints, including a 95 GeV light Higgs boson*, *Phys. Rev. D* **110** (2024) 055004 [[2405.01132](#)].
- [18] S. Khan, J. Kim and H.M. Lee, *Higgs-portal vector dark matter at a low reheating temperature*, [2503.17621](#).
- [19] B. Barman, S. Bhattacharya, S.K. Patra and J. Chakraborty, *Non-Abelian Vector Boson Dark Matter, its Unified Route and signatures at the LHC*, *JCAP* **12** (2017) 021 [[1704.04945](#)].
- [20] A. Biswas, S. Choubey, L. Covi and S. Khan, *Common origin of baryon asymmetry, dark matter and neutrino mass*, *JHEP* **05** (2019) 193 [[1812.06122](#)].
- [21] L. Covi, S. Dey, S. Khan and S.K. Rai, *Multicomponent Dark Matter with Collider Implications*, [2504.09632](#).
- [22] A. Belyaev, A. Deandrea, S. Moretti, L. Panizzi, D.A. Ross and N. Thongyoi, *Fermionic portal to vector dark matter from a new gauge sector*, *Phys. Rev. D* **108** (2023) 095001 [[2204.03510](#)].
- [23] N. Das, T. Jha and D. Nanda, *Vector dark matter with Higgs portal in type II seesaw framework*, *Phys. Rev. D* **109** (2024) 115020 [[2402.01317](#)].
- [24] G.C. Branco, P.M. Ferreira, L. Lavoura, M.N. Rebelo, M. Sher and J.P. Silva, *Theory and phenomenology of two-Higgs-doublet models*, *Phys. Rept.* **516** (2012) 1 [[1106.0034](#)].
- [25] J.F. Gunion and H.E. Haber, *Conditions for CP-violation in the general two-Higgs-doublet model*, *Phys. Rev. D* **72** (2005) 095002 [[hep-ph/0506227](#)].
- [26] L. Lopez Honorez, E. Nezri, J.F. Oliver and M.H.G. Tytgat, *The Inert Doublet Model: An Archetype for Dark Matter*, *JCAP* **02** (2007) 028 [[hep-ph/0612275](#)].
- [27] G. Arcadi, *2HDM portal for Singlet-Doublet Dark Matter*, *Eur. Phys. J. C* **78** (2018) 864 [[1804.04930](#)].
- [28] W. Chao and M.J. Ramsey-Musolf, *Hidden from view: Neutrino masses, dark matter, and tev-scale leptogenesis in a neutrinophilic two-higgs-doublet model*, *Phys. Rev. D* **89** (2014) 033007.
- [29] G. Arcadi, M. Lindner, F.S. Queiroz, W. Rodejohann and S. Vogl, *Pseudoscalar mediators: a wimp model at the neutrino floor*, *Journal of Cosmology and Astroparticle Physics* **2018** (2018) 042.

- [30] D.A. Camargo, M.D. Campos, T.B. de Melo and F.S. Queiroz, *A two higgs doublet model for dark matter and neutrino masses*, *Physics Letters B* **795** (2019) 319.
- [31] P.K. Das, S. Dey, S. Kundu and S.K. Rai, *Revisiting the inert scalar dark matter with vector-like quarks*, *JHEP* **05** (2025) 027 [[2412.17719](#)].
- [32] X.-M. Jiang, C. Cai, Z.-H. Yu, Y.-P. Zeng and H.-H. Zhang, *Pseudo-nambu-goldstone dark matter and two-higgs-doublet models*, *Phys. Rev. D* **100** (2019) 075011.
- [33] T. Biekötter, P. Gabriel, M.O. Olea-Romacho and R. Santos, *Direct detection of pseudo-Nambu-Goldstone dark matter in a two Higgs doublet plus singlet extension of the SM*, *JHEP* **10** (2022) 126 [[2207.04973](#)].
- [34] X.-M. Jiang, C. Cai, Y.-H. Su and H.-H. Zhang, *Freeze-in Production of Pseudo-Nambu-Goldstone Dark Matter Model with a Real Scalar*, [2302.02418](#).
- [35] T. Biekötter and M.O. Olea-Romacho, *Reconciling Higgs physics and pseudo-Nambu-Goldstone dark matter in the S2HDM using a genetic algorithm*, *JHEP* **10** (2021) 215 [[2108.10864](#)].
- [36] C. Bonilla, D. Sokolowska, N. Darvishi, J.L. Diaz-Cruz and M. Krawczyk, *IDMS: Inert Dark Matter Model with a complex singlet*, *J. Phys. G* **43** (2016) 065001 [[1412.8730](#)].
- [37] A. Goudelis, B. Herrmann and O. Stål, *Dark matter in the Inert Doublet Model after the discovery of a Higgs-like boson at the LHC*, *JHEP* **09** (2013) 106 [[1303.3010](#)].
- [38] E.M. Dolle and S. Su, *Inert dark matter*, *Phys. Rev. D* **80** (2009) 055012.
- [39] A. Arhrib, R. Benbrik, M. El Kacimi, L. Rahili and S. Semlali, *Extended Higgs sector of 2HDM with real singlet facing LHC data*, *Eur. Phys. J. C* **80** (2020) 13 [[1811.12431](#)].
- [40] A. Dey, J. Lahiri and B. Mukhopadhyaya, *LHC signals of a heavy doublet Higgs as dark matter portal: cut-based approach and improvement with gradient boosting and neural networks*, *JHEP* **09** (2019) 004 [[1905.02242](#)].
- [41] J. Dutta, G. Moortgat-Pick and M. Schreiber, *Phenomenology of the dark matter sector in the 2HDM extended with complex scalar singlet*, *Eur. Phys. J. Plus* **140** (2025) 87 [[2203.05509](#)].
- [42] J. Herms, S. Jana, V.P. K. and S. Saad, *Minimal Realization of Light Thermal Dark Matter*, *Phys. Rev. Lett.* **129** (2022) 091803 [[2203.05579](#)].
- [43] J. Dutta, J. Lahiri, C. Li, G. Moortgat-Pick, S.F. Tabira and J.A. Ziegler, *Dark matter phenomenology in 2HDMS in light of the 95 GeV excess*, *Eur. Phys. J. C* **84** (2024) 926 [[2308.05653](#)].
- [44] J. Dutta, J. Lahiri, C. Li, G. Moortgat-Pick, S.F. Tabira and J.A. Ziegler, *Search for Dark Matter in 2HDMS at LHC and future Lepton Colliders*, [2504.14529](#).
- [45] W. Abdallah, A.K. Barik, S.K. Rai and T. Samui, *Heavy neutrino as dark matter in a neutrinophilic U(1) model*, *Eur. Phys. J. C* **84** (2024) 1087 [[2405.15333](#)].

- [46] Y. Cai and T. Li, *Singlet dark matter in a type II two Higgs doublet model*, *Phys. Rev. D* **88** (2013) 115004 [[1308.5346](#)].
- [47] C.-F. Chang, X.-G. He and J. Tandean, *Two-Higgs-Doublet-Portal Dark-Matter Models in Light of Direct Search and LHC Data*, *JHEP* **04** (2017) 107 [[1702.02924](#)].
- [48] S. Heinemeyer, C. Li, F. Lika, G. Moortgat-Pick and S. Paasch, *Phenomenology of a 96 GeV Higgs boson in the 2HDM with an additional singlet*, *Phys. Rev. D* **106** (2022) 075003 [[2112.11958](#)].
- [49] E. Ma, *Inception of Self-Interacting Dark Matter with Dark Charge Conjugation Symmetry*, *Phys. Lett. B* **772** (2017) 442 [[1704.04666](#)].
- [50] K. Kannike, *Vacuum Stability Conditions From Copositivity Criteria*, *Eur. Phys. J. C* **72** (2012) 2093 [[1205.3781](#)].
- [51] BABAR COLLABORATION collaboration, *Precision Measurement of the $B \rightarrow X_s \gamma$ Photon Energy Spectrum, Branching Fraction, and Direct CP Asymmetry $A_{CP}(B \rightarrow X_{s+d} \gamma)$* , *Phys.Rev.Lett.* **109** (2012) 191801 [[1207.2690](#)].
- [52] LHCb COLLABORATION collaboration, *Measurement of the $B_s^0 \rightarrow \mu^+ \mu^-$ branching fraction and search for $B^0 \rightarrow \mu^+ \mu^-$ decays at the LHCb experiment*, *Phys.Rev.Lett.* **111** (2013) 101805 [[1307.5024](#)].
- [53] CMS COLLABORATION collaboration, *Measurement of the $B(s)$ to $mu+$ $mu-$ branching fraction and search for B^0 to $mu+$ $mu-$ with the CMS Experiment*, *Phys.Rev.Lett.* **111** (2013) 101804 [[1307.5025](#)].
- [54] BELLE-II collaboration, *Measurement of $B^+ \rightarrow \tau^+ \nu_\tau$ branching fraction with a hadronic tagging method at Belle II*, [2502.04885](#).
- [55] F. Mahmoudi and O. Stal, *Flavor constraints on the two-Higgs-doublet model with general Yukawa couplings*, *Phys. Rev. D* **81** (2010) 035016 [[0907.1791](#)].
- [56] T. Enomoto and R. Watanabe, *Flavor constraints on the Two Higgs Doublet Models of Z_2 symmetric and aligned types*, *JHEP* **05** (2016) 002 [[1511.05066](#)].
- [57] A. Arbey, F. Mahmoudi, O. Stal and T. Stefaniak, *Status of the Charged Higgs Boson in Two Higgs Doublet Models*, *Eur. Phys. J. C* **78** (2018) 182 [[1706.07414](#)].
- [58] BABAR collaboration, *Precision Measurement of the $B \rightarrow X_s \gamma$ Photon Energy Spectrum, Branching Fraction, and Direct CP Asymmetry $A_{CP}(B \rightarrow X_{s+d} \gamma)$* , *Phys. Rev. Lett.* **109** (2012) 191801 [[1207.2690](#)].
- [59] ALEPH, DELPHI, L3, OPAL, LEP collaboration, *Search for Charged Higgs bosons: Combined Results Using LEP Data*, *Eur. Phys. J. C* **73** (2013) 2463 [[1301.6065](#)].
- [60] ATLAS collaboration, *Measurement of the Higgs boson mass in the $H \rightarrow ZZ^* \rightarrow 4\ell$ decay channel with $\sqrt{s} = 13$ TeV pp collisions using the ATLAS detector at the LHC*, .
- [61] ATLAS collaboration, *Combination of searches for invisible decays of the Higgs*

- boson using 139 fb^{-1} of proton-proton collision data at $s=13\text{ TeV}$ collected with the ATLAS experiment, *Phys. Lett. B* **842** (2023) 137963 [[2301.10731](#)].
- [62] CMS collaboration, *A search for decays of the Higgs boson to invisible particles in events with a top-antitop quark pair or a vector boson in proton-proton collisions at $\sqrt{s} = 13\text{ TeV}$* , *Eur. Phys. J. C* **83** (2023) 933 [[2303.01214](#)].
- [63] ATLAS collaboration, *Summary plots for beyond Standard Model Higgs boson benchmarks for direct and indirect searches*, .
- [64] PARTICLE DATA GROUP collaboration, *Review of Particle Physics*, *PTEP* **2020** (2020) 083C01.
- [65] W. Grimus, L. Lavoura, O.M. Ogreid and P. Osland, *A Precision constraint on multi-Higgs-doublet models*, *J. Phys. G* **35** (2008) 075001 [[0711.4022](#)].
- [66] W. Grimus, L. Lavoura, O.M. Ogreid and P. Osland, *The Oblique parameters in multi-Higgs-doublet models*, *Nucl. Phys. B* **801** (2008) 81 [[0802.4353](#)].
- [67] A. Belyaev, N.D. Christensen and A. Pukhov, *CalcHEP 3.4 for collider physics within and beyond the Standard Model*, *Comput. Phys. Commun.* **184** (2013) 1729 [[1207.6082](#)].
- [68] G. Belanger, F. Boudjema, A. Pukhov and A. Semenov, *MicrOMEGAs 2.0: A Program to calculate the relic density of dark matter in a generic model*, *Comput. Phys. Commun.* **176** (2007) 367 [[hep-ph/0607059](#)].
- [69] L.J. Hall, K. Jedamzik, J. March-Russell and S.M. West, *Freeze-In Production of FIMP Dark Matter*, *JHEP* **03** (2010) 080 [[0911.1120](#)].
- [70] D. Gilman, S. Birrer, A. Nierenberg, T. Treu, X. Du and A. Benson, *Warm dark matter chills out: constraints on the halo mass function and the free-streaming length of dark matter with eight quadruple-image strong gravitational lenses*, *Mon. Not. Roy. Astron. Soc.* **491** (2020) 6077 [[1908.06983](#)].
- [71] V. Iršič, M. Viel, M.G. Haehnelt, J.S. Bolton, M. Molaro, E. Puchwein et al., *Unveiling dark matter free streaming at the smallest scales with the high redshift lyman-alpha forest*, *Phys. Rev. D* **109** (2024) 043511.